Chinese Journal of Astronomy and Astrophysics manuscript no.
(LaTeX: parameters˙wind.tex; printed on February 2, 2008; 7:44)

Afterglow Light Curves of Jetted Gamma-ray Burst Ejecta in Stellar Winds

Xue-Feng Wu ⋆, Zi-Gao Dai, Yong-Feng Huang and Hai-Tao Ma

Department of Astronomy, Nanjing University, Nanjing 210093, China

Received 2004 February 26; accepted 2004 May 9

Abstract Optical and radio afterglows arising from the shocks by relativistic conical ejecta running into pre-burst massive stellar winds are revisited. Under the homogeneous thin-shell approximation and a realistic treatment for the lateral expansion of jets, our results show that a notable break exists in the optical light curve in most cases we calculated in which the physical parameters are varied within reasonable ranges. For a relatively tenuous wind which cannot decelerate the relativistic jet to cause a light curve break within days, the wind termination shock due to the ram pressure of the surrounding medium occurs at a small radius, namely, a few times 10^{17} cm. In such a structured wind environment, the jet will pass through the wind within several hours and run into the outer uniform dense medium. The resulting optical light curve flattens with a shallower drop after the jet encounters the uniform medium, and then declines deeply, triggered by runaway lateral expansion.

Key words: hydrodynamics – relativity – shock waves – gamma-rays: bursts

1 INTRODUCTION

Gamma-ray Bursts (GRBs) are becoming gradually understood since the *Beppo*SAX afterglow era (Piran 1999; van Paradijs, Kouveliotou & Wijers 2000; Cheng & Lu 2001; Mészáros 2002). Standard afterglow models have been set up within the hydrodynamical context of relativistic external shocks of spherical explosions running into either interstellar medium (Sari, Piran & Narayan 1998) or stellar winds (Chevalier & Li 2000), with synchrotron emission as the main radiation mechanism. Granot & Sari (2002) have obtained more accurate results by using the well-known Blandford & McKee (1976) self-similar inner structure of relativistic blastwave instead of the thin shell approximation.

⋆ E-mail: xfwu@nju.edu.cn

However, the famous energy crisis under isotropic assumption (Kulkarni et al. 1999), together with the sharp decline of some well observed optical afterglows led to the conjecture of a jet-like form of this phenomenon (Rhoads 1997; Sari, Piran & Halpern 1999). Because of the relativistic beaming effect, the early afterglow from a jet is no different from a spherical blastwave. As the jet decelerates and the beaming effect weakens, the whole surface of the jet unfolds to the observer and the light curve declines more deeply with the decreasing radiating extent compared to the spherical blastwave. Additionally, the jet will decelerate much more rapidly when a significant or runaway lateral expansion takes place. Based on the homogeneous thin shell assumption, many authors have numerically studied jet dynamics and the behavior of the afterglow light curve (Panaitescu, Mészáros & Rees 1998; Huang et al. 2000a; Huang, Dai & Lu 2000b; Moderski, Sikora & Bulik 2000). Tremendous efforts have been devoted to the fitting of the GRB afterglows of interest (Panaitescu & Kumar 2001, 2002). The jet kinetic energy is found to be surprisingly similar in different bursts, being tightly clustered around 3×10^{50} erg. Frail et al. (2001) found the genuine gamma-ray energy releases are also clustered around 5×10^{50} erg after the jet initial aperture $\theta_{\rm j}$ inferred from afterglows are accounted for (a factor of 3 is amplified by Bloom, Frail & Kulkarni 2003). The total energy budget of a GRB is therefore close to that of a common supernova. Late time X-ray luminosity has been recognized to be largely independent of the types of environment (Kumar 2000; Freedman & Waxman 2001). Subsequent statistics of the X-ray luminosities of several GRBs at 10 hours since bursts led to the conclusion that $L_{\rm X,10hr}$ corrected by the jet aperture is again clustered around $10^{44} - 10^{45}$ erg s^{-1} (Berger, Kulkarni & Frail 2003a). The above three independent estimations all identify the GRB as a standard energy reservoir and hence as a possible probe to the Universe.

The discovery of optical transient of GRB 030329 (Price et al. 2003) and its association with SN 2003dh (Stanek et al. 2003) provides strong evidence for GRB-Supernova connection and removes any lingering doubt on the association of GRB 980425 with SN 1998bw. These two associations together with several GRBs with late time re-brightening strongly imply near simultaneity of GRBs and SNe, with trigger time difference no more than 1 to 2 days (Wu et al 2003; Hjorth et al. 2003). Although the detailed physical processes are still uncertain, the central engine of at least long GRBs has thus been confirmed to be the core collapse of massive stars, called collapsars by Woosley (1993) as well as hypernovae for their energetics by Paczyński (1998). Previous studies favored the interstellar medium (ISM) as the environment of GRBs, albeit there were indications of wind environment for several GRBs within the spherical wind interaction model (Dai & Lu 1998b; Mészáros, Rees & Wijers 1998; Chevalier & Li 1999, 2000; Li & Chevalier 1999, 2001, 2003; Dai & Wu 2003). The preference is partly due to the conclusion, based on the previous works (Kumar & Panaitescu 2000; Gou et al. 2001), that a jet in a stellar wind cannot produce a sharp break in the light curve. In fact, radiative loss of jet

energy was improperly neglected in these works, because the radiative phase lasts for hours or even one day due to the large wind density in the early afterglow. This fast cooling radiation will reduce the jet energy by about one order of magnitude. Realistic jets with energy losses in the stellar wind environments are found to be consistent with several GRB afterglows (Panaitescu & Kumar 2002). Another origin of the bias against the wind environment arises from the relatively large χ^2 or even impossibility of fit in some bursts. This result may be understood if the complicated mass loss evolutions of the progenitors at different stages and their interactions with larger scale environments are taken into account (Chevalier 2003). However, the region near the progenitor (within sub-pc) will not be affected and will be reflected in the intra-day afterglow. Even in the case of a supernova taking place 2 days earlier than the associated GRB, the supernova ejecta moving with one tenth of the light speed will reach no more than 10^{16} cm, which is the typical deceleration radius marking the beginning of the afterglows.

According to the above review of the recent progress of the GRBs and the wind environment, it seems worthwhile to revisit the evolution and radiation of homogeneous jets in a stellar wind environment. In this paper, we will study the dynamics and radiation in the jet plus wind model in Section 2. Numerical results with afterglow light curves clarifying the effects of different parameters are presented in Section 3. In Section 4 we give our discussion and conclusions.

2 DYNAMICS AND RADIATION

The dynamics of a realistic jet with radiative loss and lateral expansion running into a homogeneous interstellar medium is well described in Huang, Dai & Lu (2000b) and Huang et al. (2000a). Gou et al. (2001) studied in detail the evolution of a jet in a stellar wind environment, but they did not consider the radiative loss. We will follow these works and consider the radiative loss which is especially important in the wind environment case. We will also extend our calculation of the light curves into the radio band. Here we first give a brief description of our improved model.

2.1 Dynamics

The evolution of the radius R, swept-up mass m, half-opening angle θ and Lorentz factor γ of the beamed GRB ejecta with initial baryon loading $M_{\rm ej}$ and Lorentz factor γ_0 is described by (Huang et al. 2000a; Huang, Dai & Lu 2000b)

$$\frac{{\rm d}R}{{\rm d}t} = \beta c\gamma(\gamma + \sqrt{\gamma^2 - 1}), \tag{1}$$

$$\frac{{\rm d}m}{{\rm d}R} = 2\pi R^2(1 - \cos\theta)nm_{\rm p}, \tag{2}$$

$$\frac{{\rm d}\theta}{{\rm d}t} = \frac{c_{\rm s}(\gamma + \sqrt{\gamma^2 - 1})}{R}, \tag{3}$$

$$\frac{\mathrm{d}\gamma}{\mathrm{d}m} = -\frac{\gamma^2 - 1}{M_{\rm ej} + \epsilon m + 2(1-\epsilon)\gamma m}, \tag{4}$$

where t is the observer's time, $\beta = \sqrt{\gamma^2 - 1}/\gamma$, n is the proton number density of the surrounding medium, m_p is the mass of a proton, and ϵ is the radiative efficiency. For a stellar wind environment, the number density is given by (Chevalier & Li 1999, 2000)

$$n = AR^{-2}, \tag{5}$$

where $A = \dot{M}/4\pi m_p v_w = 3 \times 10^{35} A_*$ cm^{-1}, with $\dot{M}$ being the mass loss rate and

$$A_* = \frac{\dot{M}}{10^{-5} M_\odot \mathrm{yr}^{-1}} (\frac{v_w}{10^3 \mathrm{km\ s}^{-1}})^{-1} \tag{6}$$

is the wind parameter. The comoving sound speed $c_{\rm s}$ is (Huang et al. 2000),

$$c_{\rm s}^2 = \hat{\gamma}(\hat{\gamma} - 1)(\gamma - 1)\frac{1}{1 + \hat{\gamma}(\gamma - 1)} c^2, \tag{7}$$

where $\hat{\gamma} \approx (4\gamma + 1)/(3\gamma)$ is the adiabatic index, which is appropriate for both relativistic and non-relativistic equation of state (Dai, Huang & Lu 1999).

To estimate the radiative efficiency ϵ, we assume the shock-accelerated electrons and the amplified magnetic field in the ejecta comoving frame carry a constant fraction, $\xi_{\rm e}$ and $\xi_{\rm B}$, of the total thermal energy. The magnetic energy density and the minimum Lorentz factor of the shock accelerated power law electrons in the comoving frame are then determined by

$$\frac{B'^2}{8\pi} = \xi_{\rm B} \frac{\hat{\gamma}\gamma + 1}{\hat{\gamma} - 1} (\gamma - 1) n m_{\rm p} c^2, \tag{8}$$

$$\gamma_{\rm m} = \xi_{\rm e} (\gamma - 1) \frac{m_{\rm p}(p-2)}{m_{\rm e}(p-1)} + 1, \tag{9}$$

$m_{\rm e}$ being the electron mass and p, the index in the electron power law energy distribution. The radiative efficiency of the ejecta is determined by a combination of the available fraction of energy to radiation contained in the electrons and the efficiency of the radiation mechanisms (Dai et al. 1999),

$$\epsilon = \xi_{\rm e} \frac{t'^{-1}_{\rm syn}}{t'^{-1}_{\rm syn} + t'^{-1}_{\rm ex}}, \tag{10}$$

where $t'_{\rm ex} = R/(\gamma c)$ and $t'_{\rm syn} = 6\pi m_{\rm e} c/(\sigma_{\rm T} B'^2 \gamma_{\rm m})$ are the comoving-frame expansion time and synchrotron cooling time, respectively.

2.2 Synchrotron radiation and self-absorption

The distribution of electrons newly accelerated by the shock is assumed to be a power law function of the electron kinetic energy. Recently Huang & Cheng (2003) stressed that the distribution function should take the following form, $dN'_{\rm e}/d\gamma_{\rm e} \propto (\gamma_{\rm e} - 1)^{-p}$ with $\gamma_{\rm m} \leq \gamma_{\rm e} \leq \gamma_{\rm M}$, where $\gamma_{\rm M} = 10^8 (B'/1{\rm G})^{-1/2}$. This is especially important in the deep Newtonian stage. Radiation will cool down the electrons and thus change the shape of

the distribution. The cooling effect is significant for electrons with Lorentz factors above the critical value (Sari, Piran & Narayan 1998),

$$\gamma_{\rm c} = \frac{6\pi m_{\rm e} c}{\sigma_{\rm T}\gamma B'^2 t}. \tag{11}$$

In the comoving frame, the synchrotron radiation power at frequency ν' from electrons of known distribution is given by (Rybicki & Lightman 1979)

$$P'(\nu') = \frac{\sqrt{3}q_{\rm e}^3 B'}{m_{\rm e}c^2}\int_{\min(\gamma_{\rm m},\gamma_{\rm c})}^{\gamma_{\rm M}} (\frac{{\rm d}N'_{\rm e}}{{\rm d}\gamma_{\rm e}})F(\frac{\nu'}{\nu'_{\rm e}}){\rm d}\gamma_{\rm e}, \tag{12}$$

where $q_{\rm e}$ is the electron charge, $\nu'_{\rm e} = 3\sin\vartheta\gamma_{\rm e}^2 q_{\rm e}B'/4\pi m_{\rm e}c$ is the typical emission frequency of the $\gamma_{\rm e}$ electron, and

$$F(x) = x\int_x^\infty K_{5/3}(k){\rm d}k, \tag{13}$$

with $K_{5/3}(k)$ the Bessel function. As emphasized by Wijers & Galama (1999), the random pitch angle ϑ between the velocity of the electron and the magnetic field will have some effects on the modelling of GRB afterglows. We choose the isotropic distribution of ϑ and have

$$\nu'_{\rm e} = \frac{3\gamma_{\rm e}^2 q_{\rm e}B'}{16 m_{\rm e}c}. \tag{14}$$

The characteristic frequencies corresponding to $\gamma_{\rm c}$, $\gamma_{\rm m}$ and $\gamma_{\rm M}$ electrons are denoted by $\nu'_{\rm c}$, $\nu'_{\rm m}$ and $\nu'_{\rm M}$.

In the wind environment the early radio afterglow flux density is reduced significantly by synchrotron self absorption (SSA). This effect can be calculated by the analytical expressions derived by Wu et al. (2003). We give the more direct and convenient formula for the optical depth by SSA in different electron distributions as follows:

1. For $1 \le \gamma_{\rm c} \le \gamma_{\rm m}$,

$$\frac{{\rm d}N'_{\rm e}}{{\rm d}\gamma_{\rm e}} = \begin{cases} C_0(\gamma_{\rm e}-1)^{-2} & (\gamma_{\rm c} \le \gamma_{\rm e} < \gamma_{\rm m}), \\ C_1(\gamma_{\rm e}-1)^{-(p+1)} & (\gamma_{\rm m} \le \gamma_{\rm e} \le \gamma_{\rm M}), \end{cases} \tag{15}$$

where

$$C_0 = [(\frac{1}{\gamma_{\rm c}-1} - \frac{1}{\gamma_{\rm m}-1}) + \frac{1}{p(\gamma_{\rm m}-1)}(1 - \frac{(\gamma_{\rm m}-1)^p}{(\gamma_{\rm M}-1)^p})]^{-1} N_{\rm ele}, \tag{16}$$

$$C_1 = C_0(\gamma_{\rm m}-1)^{p-1}, \tag{17}$$

and $N_{\rm ele}$ is the total electron number of a jet element. The self-absorption optical depth is

$$\tau_{\nu'} = c_{\rm sa}\frac{q_{\rm e}}{B'}C_0\frac{N_{\rm col}}{N_{\rm ele}}\times \begin{cases} \gamma_{\rm c}^{-6}(\frac{\nu'}{\nu'_{\rm c}})^{-5/3} & (\nu' \le \nu'_{\rm c}), \\ \gamma_{\rm c}^{-6}(\frac{\nu'}{\nu'_{\rm c}})^{-3} & (\nu'_{\rm c} < \nu' \le \nu'_{\rm m}), \\ \gamma_{\rm m}^{-6}(\frac{\nu'}{\nu'_{\rm m}})^{-(p+5)/2} & (\nu'_{\rm m} < \nu' \le \nu'_{\rm M}), \\ \gamma_{\rm m}^{-6}(\frac{\nu'}{\nu'_{\rm m}})^{-5/2}(\frac{\gamma_{\rm m}}{\gamma_{\rm M}})^p e^{1-\nu'/\nu'_{\rm M}} & (\nu'_{\rm M} < \nu'), \end{cases} \tag{18}$$

where $c_{\rm sa}$ is (Wu et al. 2003)

$$c_{\rm sa} = 10.4(p+2)/(p+2/3), \tag{19}$$

while

$$N_{\rm col} = \frac{m}{2\pi(1-\cos\theta)R^2 m_{\rm p}} \tag{20}$$

is the column density through which the synchrotron photons will experience synchrotron self absorption before emerging from the jet surface. We do not consider here the corresponding correction on the optical depth by the exact distribution of electrons, since the SSA coefficients are deduced under the assumption of soft photons and ultra-relativistic electrons, and when the bulk of the electrons are in the non-relativistic region the emitting source has already been optically thin to SSA.

2. For $\gamma_{\rm m} < \gamma_{\rm c} \leq \gamma_{\rm M}$,

$$\frac{{\rm d}N'_{\rm e}}{{\rm d}\gamma_{\rm e}} = \begin{cases} C_2(\gamma_{\rm e}-1)^{-p} & (\gamma_{\rm m} \leq \gamma_{\rm e} < \gamma_{\rm c}), \\ C_3(\gamma_{\rm e}-1)^{-(p+1)} & (\gamma_{\rm c} \leq \gamma_{\rm e} \leq \gamma_{\rm M}), \end{cases} \tag{21}$$

where (Huang & Cheng 2003)

$$C_2 = C_3/(\gamma_{\rm c}-1), \tag{22}$$

$$C_3 = [\frac{(\gamma_{\rm m}-1)^{1-p} - (\gamma_{\rm c}-1)^{1-p}}{(\gamma_{\rm c}-1)(p-1)} + \frac{(\gamma_{\rm c}-1)^{-p} - (\gamma_{\rm M}-1)^{-p}}{p}]^{-1} N_{\rm ele}. \tag{23}$$

The optical depth is

$$\tau_{\nu'} = c_{\rm sa}\frac{q_{\rm e}}{B'}C_2\frac{N_{\rm col}}{N_{\rm ele}} \times \begin{cases} \gamma_{\rm m}^{-(p+4)}(\frac{\nu'}{\nu'_{\rm m}})^{-5/3} & (\nu' \leq \nu'_{\rm m}), \\ \gamma_{\rm m}^{-(p+4)}(\frac{\nu'}{\nu'_{\rm m}})^{-(p+4)/2} & (\nu'_{\rm m} < \nu' \leq \nu'_{\rm c}), \\ \gamma_{\rm c}^{-(p+4)}(\frac{\nu'}{\nu'_{\rm c}})^{-(p+5)/2} & (\nu'_{\rm c} < \nu' \leq \nu'_{\rm M}), \\ \gamma_{\rm c}^{-(p+4)}(\frac{\nu'}{\nu'_{\rm c}})^{-5/2}(\frac{\gamma_{\rm c}}{\gamma_{\rm M}})^{p} e^{1-\nu'/\nu'_{\rm M}} & (\nu'_{\rm M} < \nu'). \end{cases} \tag{24}$$

3. For $\gamma_{\rm c} > \gamma_{\rm M}$, we have

$$\frac{{\rm d}N'_{\rm e}}{{\rm d}\gamma_{\rm e}} = C_4(\gamma_{\rm e}-1)^{-p} \quad (\gamma_{\rm m} \leq \gamma_{\rm e} \leq \gamma_{\rm M}), \tag{25}$$

where (Huang & Cheng 2003)

$$C_4 = \frac{p-1}{(\gamma_{\rm m}-1)^{1-p} - (\gamma_{\rm M}-1)^{1-p}} N_{\rm ele}. \tag{26}$$

The optical depth is

$$\tau_{\nu'} = c_{\rm sa}\frac{q_{\rm e}}{B'}C_4\frac{N_{\rm col}}{N_{\rm ele}} \times \begin{cases} \gamma_{\rm m}^{-(p+4)}(\frac{\nu'}{\nu'_{\rm m}})^{-5/3} & (\nu' \leq \nu'_{\rm m}), \\ \gamma_{\rm m}^{-(p+4)}(\frac{\nu'}{\nu'_{\rm m}})^{-(p+4)/2} & (\nu'_{\rm m} < \nu' \leq \nu'_{\rm M}), \\ \gamma_{\rm m}^{-(p+4)}(\frac{\nu'}{\nu'_{\rm m}})^{-5/2}(\frac{\gamma_{\rm m}}{\gamma_{\rm M}})^{p-1} e^{1-\nu'/\nu'_{\rm M}} & (\nu'_{\rm M} < \nu'). \end{cases} \tag{27}$$

The radiation power is assumed to be isotropic in the comoving frame. Let Θ be the angle between the velocity of an emitting element and the line of sight and define $\mu = \cos\Theta$, the observed flux density at frequency ν from this emitting element is

$$S_\nu = \frac{1+z}{\gamma^3(1-\beta\mu)^3}\frac{1}{4\pi D_{\rm L}^2(z)}\frac{1-\exp(-\tau[\gamma(1-\beta\mu)(1+{\rm z})\nu])}{\tau[\gamma(1-\beta\mu)(1+z)\nu]}P'[\gamma(1-\beta\mu)(1+z)\nu], \quad (28)$$

where the luminosity distance is

$$D_{\rm L}(z) = (1+z)\frac{c}{H_0}\int_0^z \frac{dz'}{\sqrt{\Omega_{\rm M}(1+z')^3+\Omega_\Lambda}}, \quad (29)$$

with $\Omega_{\rm M} = 0.3$, $\Omega_\Lambda = 0.7$ and $H_0 = 65$ km/s/Mpc adopted in our calculations. The total observed flux density can be integrated over the equal arrival time surface determined by

$$t_{\rm obs} = (1+z)t = (1+z)\int \frac{1-\beta\mu}{\beta c}{\rm d}R \equiv {\rm const.} \quad (30)$$

3 NUMERICAL RESULTS

We investigate the effects of various parameters on the afterglow light curve in our realistic jet+wind model. For convenience, we chose a set of 'standard' initial parameters as follows: $E_{\rm iso} = 2\times10^{53}$ erg, $\theta_0 = 0.1$, $\theta_{\rm v} = 0$, $\gamma_0 = 300$, $\xi_{\rm e} = 0.1$, $\xi_{\rm B} = 0.1$, $p = 2.2$, and $A_* = 1.0$. θ_0 is the jet half-opening angle while $\theta_{\rm v}$ is the observer's viewing angle with respect to the jet axis. The GRB in our calculations is assumed to be at $z = 1$, and the luminosity distance is about $D_{\rm L} = 7.1$ Gpc.

Figure 1 shows the optical and radio light curves with $E_{\rm iso}$ varying between 10^{52} and 10^{54} erg while the other parameters are fixed at their standard values. The early optical light curves resemble roughly those of spherical ones (for analytical jet+wind model, see Livio & Waxman 2000). The theoretical temporal evolution of the optical flux density changes from $t^{-1/4}$ to $t^{-(3p-2)/4}$ ($t^{-1.15}$ for $p = 2.2$) when $\nu_{\rm m}$ crosses the optical band, at time (Chevalier & Li 2000)

$$t_{\rm m} = 0.1(\frac{1+z}{2})^{1/3}(\frac{\xi_{\rm e}}{0.1})^{4/3}(\frac{\xi_{\rm B}}{0.1})^{1/3}E_{\rm iso,53}^{1/3}\nu_{\rm R}^{-2/3}\ {\rm days}, \quad (31)$$

where $\nu_{\rm R} = \nu/4.36\times10^{14}$ Hz is scaled to the $R-$band frequency and where we have adopted the convention $Q = 10^{\rm x}Q_{\rm x}$. The actual indices of the light curves in our calculations deviate slightly from the ideal spherical predictions. Wei & Lu (2002a, 2002b) suggested that some sharp breaks come from a spectral origin. Nevertheless, the radiative loss of kinetic energy and the effect of equal arrival time surface (EATS) cause several differences in the temporal evolution. For the extremely high isotropic energy case, viz. $E_{\rm iso,53} = 10$, there are two breaks in the light curve, as it evolves from $t^{-0.95}$ to $t^{-1.6}$, and finally approaches the jet-like behavior $t^{-2.0}$. This temporal behavior is also seen in the 'standard' $E_{\rm iso,53} = 2$ case, except that the scaling law evolves from $t^{-1.14}$ to $t^{-1.8}$ and finally reaches $t^{-2.0}$. For other low $E_{\rm iso}$ cases, the light curves have only one break, while before the jet break the temporal index β is $\sim 1.3-1.4$ and after the jet break

$\beta \approx 2.0$ ($F_\nu \propto t^{-\beta}$). The theoretical change of β in the spherical wind model takes place at (see also, Chevalier & Li 2000)

$$t_{\rm c} = 3.8 \times 10^3 (\frac{1+z}{2})^3 (\frac{\xi_{\rm B}}{0.1})^3 E_{\rm iso,53}^{-1} A_*^4 \nu_{\rm R}^2 \ {\rm days}, \tag{32}$$

which is much later than the moment when significant lateral expansion is included. After that $\nu_{\rm c}$ will cross the R band and β changes from $(3p-2)/4$ to $(3p-1)/4$ (i.e. from 1.15 to 1.4 for $p = 2.2$). The difference of β between the jet model and the spherical model is ascribed to the EATS effect (see also Fig. 2 of Kumar & Panaitescu 2000). The radiative loss of energy also plays an important role for this diversity of the light curves. A crude estimate of the energy loss can be made by synchrotron radiation within the spherical fireball model. When the fireball is in the fast cooling stage, the observed power is $P_\oplus = -\frac{{\rm d}E_{\rm iso}}{{\rm d}t_\oplus} \approx \xi_{\rm e} \frac{E_{\rm iso}}{t_\oplus}$ and the fireball energy evolves as

$$E_{\rm iso} = E_{\rm iso,i} (\frac{t_\oplus}{t_{\rm i}})^{-\xi_{\rm e}}, \tag{33}$$

where $E_{\rm iso,i}$ is the initial energy and $t_{\rm i} = t_{\rm dec} = 1.5 \times 10^{-6} (\frac{1+z}{2}) E_{\rm iso,53} A_*^{-1} (\frac{\gamma_0}{300})^{-4}$ day is the initial time of the afterglow, which begins at the deceleration radius. The fast cooling stage ends at $t_0 = 2(\frac{1+z}{2})(\frac{\xi_{\rm e}}{0.1})(\frac{\xi_{\rm B}}{0.1}) A_*$ days (Chevalier & Li 2000). The kinetic energy decreases to $E_{\rm iso,0} \sim 0.25 E_{\rm iso,i}$ ($\xi_{\rm e} = 0.1$) at t_0. The synchrotron power in the slow cooling stage is $P_\oplus \approx \frac{\xi_{\rm e}}{3-p} (\frac{t_\oplus}{t_0})^{-(p-2)/2} \frac{E_{\rm iso}}{t_\oplus}$. The fireball energy is

$$E_{\rm iso,f} \approx E_{\rm iso,0} {\rm exp}[-\frac{2\xi_{\rm e}}{(3-{\rm p})({\rm p}-2)}] \approx 0.07 E_{\rm iso,i}, \tag{34}$$

in which we have put $p = 2.2$ and $\xi_{\rm e} = 0.1$. Early works neglected such tremendous loss of the jet energy and assumed relatively large isotropic energy and jet opening angle, leading to inconspicuous jet breaks (Gou et al. 2001). However, we show that notable breaks of optical light curves exist in all cases, as can be seen in Fig. 1. Although the temporal indices both before and after the break (see Fig. 1, t ~several$\times 10^4$ seconds) vary with $E_{\rm iso}$, the change of the temporal index in each case is nearly the same, $\Delta\beta \approx 0.65$, and is well within one decade of time. Kumar & Panaitescu (2000) found that in a stellar wind β increases by ~ 0.4 over two decades of time, while in a uniform density medium β increases by ~ 0.7 within about one decade of time. However, their conclusion is based on ignoring the energy losses by radiation. Our present results thus make the jet+wind model competitive with the jet+ISM model. Radio afterglows are affected by the synchrotron self-absorption due to the dense wind medium at early times. A rapid rise of radio flux density proportional to t^2 in Fig. 1 is consistent with theoretical expectation. As $E_{\rm iso}$ decreases, the transition to the optical thin regime becomes later than $t_{\rm m}$, and the radio light curve changes from type D to type E of Chevalier & Li (2000). At late times, the radio afterglows decay as t^{-p} because of lateral expansion.

The effect of the wind parameter A_* on the afterglow light curves is shown in Fig. 2. The early optical light curves (less than $\sim 10^3$ s) and late-time radio light curves (when

jet lateral expansion is significant) show little difference in the three cases with different A_*. The jet break in the optical band is indistinctive when $A_* = 0.3$, contrary to denser wind cases, in which an obvious optical break occurs around one day. The early radio afterglow is suppressed more strongly in denser winds. The radio light curves changes from type D to type E as A_* increases.

For a relatively tenuous wind which cannot decelerate the relativistic jet to cause a sharp break around one day, the wind termination shock due to the ram pressure balanced by the surrounding medium occurs at a small radius, i.e. several times 10^{17} cm (Ramirez-Ruiz et al. 2001). Different mass loss histories of the progenitors or different large-scale environments surrounding the winds will lead to diverse environments for the GRB afterglow (see the review by Chevalier 2003). At least four kinds of GRB environment have been considered so far, stellar wind (Dai & Lu 1998b; Mészáros et al. 1998; Chevalier & Li 1999), the ISM, dense medium (Dai & Lu 1999) and density jumps (Dai & Lu 2002). The complex, stratified medium resulting from interaction between the winds or between a wind and an outer dense medium interaction has been recently proposed to explain GRB 030226 by Dai & Wu (2003). This complicated and more realistic environment has the potential of unifying the diverse media, and, especially, of explaining the peculiar afterglow of GRB 030329 that included a large flux increase and several fluctuations. Fluctuations subtracted from the power-law light curve of GRB 021004 indicate clouds and shells around the wind of a Wolf-Rayet star, which is the progenitor of an SN Ib/c and a collapsar (Schaefer et al. 2003; Mirabal et al. 2003). In the complicated wind case, the jet will reach the wind termination shock radius at the observed time (Ramirez-Ruiz et al. 2001; Chevalier & Li 2000)

$$t_{\rm t} = 1.5(\frac{1+z}{2})A_{*,-1}^2 E_{\rm iso,53}^{-1} n_{\rm out} \ {\rm hrs}, \tag{35}$$

where $n_{\rm out}$ is the number density of the outer uniform medium in units of cm^{-3}. After this time the jet enters the outer uniform medium. We calculate the light curve of such a jet with $A_* = 0.1$ and $n_{\rm out} = 1$ cm^{-3}. The density ratio of the outer medium to the wind at the termination shock radius is ~ 4, which will not lead to a reverse shock propagating into the jet. As illustrated in Fig. 3, the resulting optical light curve flattens from an initial $t^{-1.5}$ before 6 hours to $t^{-1.2}$ after entering the uniform medium, and then declines steeply as $t^{-2.3}$ after ~ 9 days due to runaway lateral expansion. This result provides the first piece of evidence that in the tenuous wind case an obvious sharp break can be caused by the medium outside the wind termination shock. The radio flux density will increase by a factor of a few since $t_{\rm t}$ and thereafter follows the behavior of the jet+ISM model, which exhibits a jet break and shows a late time flattening when the shock becomes spherical and enters the deep Newtonian phase.

The previous estimate of the jet half-opening angle θ_0 comes from direct fitting of afterglows and observed jet break time (Panaitescu & Kumar 2001, 2002; Frail et al.

2001; Bloom et al. 2003). Statistics shows a large dispersion of θ_0, ranging from 2° to $\sim 40^\circ$. Here we calculate the effect of θ_0 on the light curves, this result is shown in Fig. 4. A large θ_0 reduces the jet edge effects. For the case of $\theta_0 = 0.2$, the temporal index β for the R band varies from 1.1 to 1.55 and then to 2.0 at ~ 100 days. However, jets with relatively smaller θ_0 will experience the jet break at earlier times. For the cases of $\theta_0 = 0.075$ and 0.05, β evolves from $1.3 - 1.4$, to 2.0 at around 1 day. The corresponding $\Delta\beta$ is 0.7 and 0.6, respectively. The radio light curves show no difference at early times, due to the relativistic beaming effect and the same energy per solid angle.

As we know, the strong correlation between $E_{\rm iso}$ and θ_0 makes the GRBs a standard candle. A reliable treatment of the effect of $E_{\rm iso}$ or θ_0 to the jet light curves should include their intrinsic connection. We calculate the afterglows under the assumption of standard energy reservoir, $E_{\rm j} \approx E_{\rm iso}\dfrac{\theta_0^2}{2} \equiv 2\times10^{51}$ erg, and illustrate the results in Fig. 5. The characteristic feature of sharp breaks still remains for the narrow jets. For the case of $\theta_0 = 0.2$, β for the R band evolves from 1.16 to 1.7, which is relative shallower than typical jet-break. The temporal index will further approach 1.86 tens of days later. For a standard candle with smaller angle of $\theta_0 = 0.05$ ($\theta_0 = 0.025$), β evolves from 1.25 (1.3) to 1.85 (1.9) and then reaches 2.05 (2.06). Comparing with Fig. 4, the light curves in Fig. 5 are more diverse at early times because the energy per solid angle is not a constant. Larger θ_0 will result in a smaller value of energy per solid angle and cause a lower level of flux density of both the optical and radio afterglows. However, the late time light curves are almost the same.

We also investigate the effects of $\xi_{\rm e}$ and $\xi_{\rm B}$ on the light curves. Their most important effect is in the jet dynamics due to radiative loss, as illustrated in Eqs. (33) and (34). Figure 6 shows the effects of $\xi_{\rm e}$ on the afterglows. In the case of $\xi_{\rm e} = 0.2$, β changes from 1.2 to 1.95. In the case of $\xi_{\rm e} = 0.4$, β changes from 1.5 to 2.2. Both cases show sharp breaks of $\Delta\beta \approx 0.7$ at around one day. The effect of $\xi_{\rm B}$ is more complicated, since changing $\xi_{\rm B}$ significantly alters the type of the optical light curve. According to Eq. (32), $t_{\rm c}$ is very sensitive to $\xi_{\rm B}$. A small $\xi_{\rm B}$ will result in a type B optical afterglow, in which $\beta = (3p-1)/4$ (Chevalier & Li 2000). The reason is that the three characteristic time scales depend on $\xi_{\rm B}$ as $t_{\rm c} \propto \xi_{\rm B}^3$, $t_0 \propto \xi_{\rm B}$ and $t_{\rm m} \propto \xi_{\rm B}^{1/3}$. Decreasing $\xi_{\rm B}$ will alter these three times significantly and lead to a type B afterglow, i.e. $t_{\rm c} < t_0 < t_{\rm m}$. Figure 7 shows that, for $\xi_{\rm B} = 10^{-2}$ and 10^{-3}, the β of the optical light curve evolves from 1.6 at early times to ~ 2.1 ten days later. Although $\Delta\beta \approx 0.5$, the break is still obvious since it is completed within one decade of time in these cases.

It is interesting to study the effect of the electron energy index, p, on the light curves. Theoretically p is very likely to lie within 2.2 - 2.4, but observations of GRB afterglows indicate that p may cover a rather wide range. Figure 8 shows the behavior of the afterglows with different p. It should be pointed out that the jet dynamics is not affected by p in our considerations. The light curves show no difference at very early times. For

the optical afterglow, β evolves from 1.28 to 2.0 and 2.25 at very late times in the case of $p = 2.4$, while from 1.48 (1.6) to 2.2 (2.4) and finally to 2.55 (2.8) in the case of $p = 2.6$ ($p = 2.8$). The former breaks with $\Delta\beta \sim 0.7$ - 0.8 are sharp enough to make the jet + wind model capable of fitting most of the observed breaks in afterglows.

It is also important to determine the jet initial Lorentz factor through fitting the afterglows. Previous works have discussed the optical flash arising from a reverse shock when a fireball shell interacts with its circum-progenitor wind (Chevalier & Li 2000; Wu et al. 2003). The Lorentz factor can be determined from the optical flash. The imprint of Lorentz factor is also expected to appear in very early afterglows. Figure 9 illustrates the difference in the early optical and radio afterglows caused by different initial Lorentz factors. We see that lower Lorentz factors give lower flux densities at early times. However, late time afterglows depend mainly on the total energy of the jet and so the light curves in Figure 9 differ from each other only slightly at late stages.

Lastly, we examine the effects of the viewing angle within our jet + wind model and illustrate the results in Fig. 10. This study may be of some help to our understanding of orphan afterglows, which are afterglows whose parent bursts are not observed because they lay off-axis with respect to our line of sight (Huang, Dai & Lu 2002).

The actual profile of GRB jets is likely to be Gaussian (Zhang & Mészáros 2002a). It is interesting that the afterglow behavior of a Gaussian jet is very similar to that of a simple uniform jet, especially when the uniform jet is assumed to have no lateral expansion. This conclusion is supported by the hydrodynamical simulations of Kumar & Granot (2003), who showed that the lateral expansion velocity (v_θ) of a Gaussian jet is significantly less than the local sound speed. In other words, we can approximate a Gaussian jet with a uniform jet with lateral expansion velocity set at $v_\theta = 0$. In Fig. 11, we illustrate the effect of v_θ on the afterglow light curves. It is clearly shown that although the absolute intensities are different, the jet breaks in the R-band light curves are similar in the both cases. In the $v_\theta = 0$ case, β evolves from 1.0 to 1.7, so that the light curve breaks by about $\Delta\beta = 0.7$ at around one day.

4 DISCUSSION AND CONCLUSIONS

The recently observed association of GRB 030329 and SN 2003dh strongly suggests a massive star origin for long GRBs. In the context of massive star evolution, a type Ib/c SN is expected to explode from a Wolf-Rayet star. The environment is thus likely to be a high speed stellar wind ejected from the progenitor. Despite the above basic physical reasoning, results of previous works favored instead an interstellar medium environment. This preference was partly due to the fact that the previous authors thought that the jet+wind model was unable to produce sharp breaks in the optical afterglow light curves. In this paper we have revisited a realistic jet+wind model and studied the effects of

various parameters, such as $E_{\rm iso}$, θ_0, A_*, $\xi_{\rm e}$, $\xi_{\rm B}$, etc.. Our more realistic model includes radiative energy loss and lateral expansion as well as the equal-arrival time surface effect. Inverse Compton scattering of synchrotron photons is not considered in this work, which can additionally decrease the cooling electron Lorentz factor $\gamma_{\rm c}$, leading to a further decrease of the jet energy. We find that obvious breaks can in fact be seen in the optical light curves. Temporal evolution of the jet energy due to radiative loss may be the main ingredient that gives rise to the notable break. Inverse Compton spectra components emerge always in the X-ray band, and will not significantly affect the temporal behavior of the optical afterglows in our calculations. Our results strongly suggest that breaks in the light curve can also be produced by jets expanding into stellar winds. The change of temporal index $\Delta\beta$ of these breaks, generally ranging from ~ 0.6 to 0.8, happens from less than a day to several days since the GRB while the transitions are generally well within one decade of time. The smallest break $\Delta\beta \approx 0.5$ in our calculation occurs in a very weak wind. In reality, the stellar wind may be surrounded by an outer homogeneous medium, which would greatly complicate the physics of afterglows.

Despite the overwhelming success of this simple jet model, the structure of GRB jets has recently been intrigued to the model constructors, although it has already been considered in early works (Mészáros et al. 1998; Dai & Gou 2001). The motivation is driven by the large dispersion of both the isotropic gamma-ray energy releases and the jet apertures, compared to their tight correlation resulting in a standard candle as discussed above. There are two simple treatments of the jet structure that keep to the axial symmetry. One common treatment is to assume the energy per solid angle and the Lorentz factor (therefore the baryon loading) decrease as power law functions of the angle from the jet axis. There exists a uniform and very narrow inner cone at the center in order to keep the total energy not finite. This kind of structured jet has the advantage of being able to explain the observed larger jet aperture with lower isotropic luminosity simply as the viewing angle effect, if the power law index of the energy distribution is about -2. It is also capable of reproducing the sharp breaks of some optical afterglows, as well as the observed luminosity function (Rossi, Lazzati & Rees 2002; Zhang & Mészáros 2002a). As the transverse gradient of energy density is much smaller in the structured jet than in the homogeneous jet which has a definite boundary with the environment, the lateral expansion almost never approaches the local sound speed in the co-moving frame and can essentially be neglected in the analytic solutions (Kumar & Granot 2003). Detailed reexamination of structured jet is now available both numerically (Kumar & Granot 2003) and analytically (Wei & Jin 2003; Granot & Kumar 2003; Panaitescu & Kumar 2003; Salmonson 2003). However, the most probable profile of power law structured jet is the one with the energy index -2 and a constant Lorentz factor, constrained by the existing afterglows (Granot & Kumar 2003). The other treatment is to assume the energy per solid angle as a Gaussian function of the angle from the jet axis (Zhang

& Mészáros 2002a; Zhang et al. 2004). This Gaussian jet, despite relatively small lateral expansion, will not deviate from the simple homogeneous jet significantly in their afterglow behaviors (Kumar & Granot 2003; Zhang & Mészáros 2002a).

Although the power law structured jet model has the potential virtue of interpreting the large dispersion of GRBs within a unified picture, it is still confronted by several difficulties. (1) It is not supported by the simulations of relativistic jet formation during the core collapsing of massive stars by MacFadyen & Woosley (2001). In their J32 model, the profile of the energy distribution at the emergence from the progenitor envelope is much better described by a Gaussian function, i.e. a Gaussian jet. In fact, the index should be -4 rather than -2 between 5° and 10° if a power law energy distribution is assumed. Zhang, Woosley & Heger (2004) have calculated the propagation of a relativistic jet within its massive stellar progenitor (see also Zhang, Woosley & MacFadyen 2003). The ultimate structure at emergence is characterized by a uniform core component of a higher Lorentz factor spanning a few degree, with a sharp decline boundary adjoining a wider component with a lower Lorentz factor. (2) The power law structured jet model unifies most GRBs at the expense of introducing another adjustable parameter, $\theta_{\rm c}$, the half-opening angle of the uniform core component. Different central engine properties will lead to different jet half-opening angle θ (MacFadyen & Woosley 2001). To maintain the merit of power law structured jet model we have to regard $\theta_{\rm c}$ as a universal constant for all GRBs, and this has to be confirmed by observations through data fitting. (3) The most probable distribution of the Lorentz factor is a homogeneous one within the jet. But it is difficult to imagine such a distribution can be sustained at large angles and not affected by abundant baryon loading outside a very narrow funnel. The homogeneous jet model also appreciably suffers from this problem for a few GRB afterglows with large apertures, and can be settled by considering a two-component model as recently proposed (Berger et al 2003b; Huang, et al. 2004). (4) Another difficulty for the power law structured jet model may be the pre-break flattening predicted by a few authors (Wei & Jin 2003; Kumar & Granot 2003; Granot & Kumar 2003). The flattening is due to the emergence of the core component before the jet break of the light curve while the observer's line of sight is outside $\theta_{\rm c}$. Such a flattening will even develop to a pre-break bump if $\theta_{\rm c}$ is within 1° (Salmonson 2003). This new type of bump has been proposed to explain the peculiar behavior of GRB 000301C, as an alternative to energy injection, density jump and microlensing scenarios (Dai & Lu 1998a; Zhang & Mészáros 2002b; Dai & Lu 2002; Garnavich, Loeb & Stanek 2000). However, it is suspect because some well-observed afterglows with large jet aperture such as GRB 000926 ($\theta_{\rm j} = 8.1^\circ$) have not shown this pre-break bump behavior (Panaitescu & Kumar 2002). Future observations of very early afterglows in the upcoming $Swift$ era would help to discriminate the structure of GRB jets. As proposed by Zhang & Mészáros (2002a), actual profiles of GRB jets may be Gaussian. The sideways expansion can be neglected since the gradients of physical

parameters in a Gaussian jet are much smaller than in an ideal uniform jet with a clear-cut lateral boundary to its environment. In such a case, a sharp break exists as well. With the self-absorption of synchrotron radiation included in our realistic jet+wind model, we are able to do broad-band fittings of observed GRB afterglows.

Acknowledgements We thank the anonymous referee for useful comments. This work was supported by the National Natural Science Foundation of China (grant numbers 10233010, 10003001, 10221001), the National 973 project (NKBRSF G19990754), the Foundation for the Authors of National Excellent Doctorial Dissertations of P. R. China (Project No: 200125) and the Special Funds for Major State Basic Research Projects.

References

Berger E., Kulkarni S. R., Frail D. A., 2003a, ApJ, 590, 379

Berger E., Kulkarni S. R., Pooley G. et al., 2003b, Nature, 426, 154

Blandford R. D., McKee C. F., 1976, Phys. Fluids, 19, 1130

Bloom J. S., Frail D. A, Kulkarni S. R., 2003, ApJ, 594, 674

Cheng K. S., Lu T., 2001, ChJAA, 1, 1

Chevalier R. A., Li Z. Y., 1999, ApJ, 520, L29

Chevalier R. A., Li Z. Y., 2000, ApJ, 536, 195

Chevalier R. A., 2003, In: J. M. Marcaide, K. W. Weiler, eds., IAU Colloq. 192, Supernovae: 10 Years of 1993J, Springer Verlag, preprint (astro-ph/0309637)

Dai Z. G., Lu T., 1998a, Phys. Rev. Lett, 81, 4301

Dai Z. G., Lu T., 1998b, MNRAS, 298, 87

Dai Z. G., Huang Y. F., Lu T., 1999, ApJ, 520, 634

Dai Z. G., Lu T., 1999, ApJ, 519, L155

Dai Z. G., Gou L. J., 2001, ApJ, 552, 72

Dai Z. G., Lu T., 2002, ApJ, 565, L87

Dai Z. G., Wu X. F., 2003, ApJ, 591, L21

Frail D. A. et al, 2001, ApJ, 562, L55

Freedman D. L., Waxman E., 2001, ApJ, 547, 922

Garnavich P. M., Loeb A., Stanek K. Z., 2000, ApJ, 544, L11

Gou L. J., Dai Z. G., Huang Y. F. et al., 2001, A&A, 368, 464

Granot J., Sari R., 2002, ApJ, 568, 820

Granot J., Kumar P., 2003, ApJ, 591, 1086

Hjorth J., Sollerman J., Moller P. et al, 2003, Nature, 423, 847

Huang Y. F., Gou L. J., Dai Z. G. et al., 2000a, ApJ, 543, 90

Huang Y. F., Dai Z. G., Lu T., 2000b, MNRAS, 316, 943

Huang Y. F., Dai Z. G., Lu T., 2002, MNRAS, 332, 735

Huang Y. F., Cheng K. S., 2003, MNRAS, 341, 263

Huang Y. F., Wu X. F., Dai Z. G. et al., 2004, ApJ, 605, 300

Kulkarni S. R., Djorgovski S. G., Odewahn S. C. et al, 1999, Nature, 398, 389

Kumar P., 2000, ApJ, 538, L125

Kumar P., Panaitescu A., 2000, ApJ, 541, L9

Kumar P., Granot J., 2003, ApJ, 591, 1075

Li Z. Y., Chevalier R. A., 1999, ApJ, 526, 716

Li Z. Y., Chevalier R. A., 2001, ApJ, 551, 940

Li Z. Y., Chevalier R. A., 2003, ApJ, 589, L69

Livio M., Waxman E., 2000, ApJ, 538, 187

MacFadyen A. I., Woosley S. E., Heger A., 2001, ApJ, 550, 410

Mészáros P., Rees M. J., Wijers R. A. M. J., 1998, ApJ, 499, 301

Mészáros P., 2002, ARA&A, 40, 137

Mirabal N., Halpern J. P., Chornock R. et al., 2003, ApJ, 595, 935

Moderski R., Sikora M., Bulik T., 2000, ApJ, 529, 151

Paczyński B., 1998, ApJ, 494, L45

Panaitescu A., Mészáros P., Rees M. J., 1998, ApJ, 503, 314

Panaitescu A., Kumar P., 2001, ApJ, 560, L49

Panaitescu A., Kumar P., 2002, ApJ, 571, 779

Panaitescu A., Kumar P., 2003, ApJ, 592, 390

Piran T., 1999, Phys. Rep., 314, 575

Price P. A., Fox D. W., Kulkarni S. R. et al., 2003, Nature, 423, 844

Ramirez-Ruiz E., Dray L. M., Madau P. et al., 2001, MNRAS, 327, 829

Rhoads J., 1997, ApJ, 487, L1

Rossi E., Lazzati D., Rees M. J., 2002, MNRAS, 332, 945

Rybicki G. B., Lightman A. P., 1979, Radiative Processes in Astrophysics, Wiley, New York

Salmonson J. D., 2003, ApJ, 592, 1002

Sari R., Piran T., Narayan R., 1998, ApJ, 497, L17

Sari R., Piran T., Halpern J. P., 1999, ApJ, 519, L17

Schaefer B. E., Gerardy C. L., Höflich P. et al., 2003, ApJ, 588, 387

Stanek K. Z., Matheson T., Garnavich P. M. et al., 2003, ApJ, 591, L17

van Paradijs J., Kouveliotou C., Wijers R. A. M. J., 2000, ARA&A, 38, 379

Wei D. M., Lu T., 2002a, MNRAS, 332, 994

Wei D. M., Lu T., 2002b, A&A, 381, 731

Wei D. M., Jin Z. P., 2003, A&A, 400, 415

Wijers R., Galama T., 1999, ApJ, 523, 177

Woosley S. E., 1993, ApJ, 405, 273

Wu X. F., Dai Z. G., Huang Y. F. et al., 2003, MNRAS, 342, 1131

Zhang B., Mészáros P., 2002a, ApJ, 571, 876

Zhang B., Mészáros P., 2002b, ApJ, 566, 712

Zhang B., Dai X., Lloyd-Ronning N. M. et al., 2004, ApJ, 601, L119

Zhang W., Woosley S. E., MacFadyen A. I., 2003, ApJ, 586, 356

Zhang W., Woosley S. E., Heger A., 2004, ApJ, 608, 365

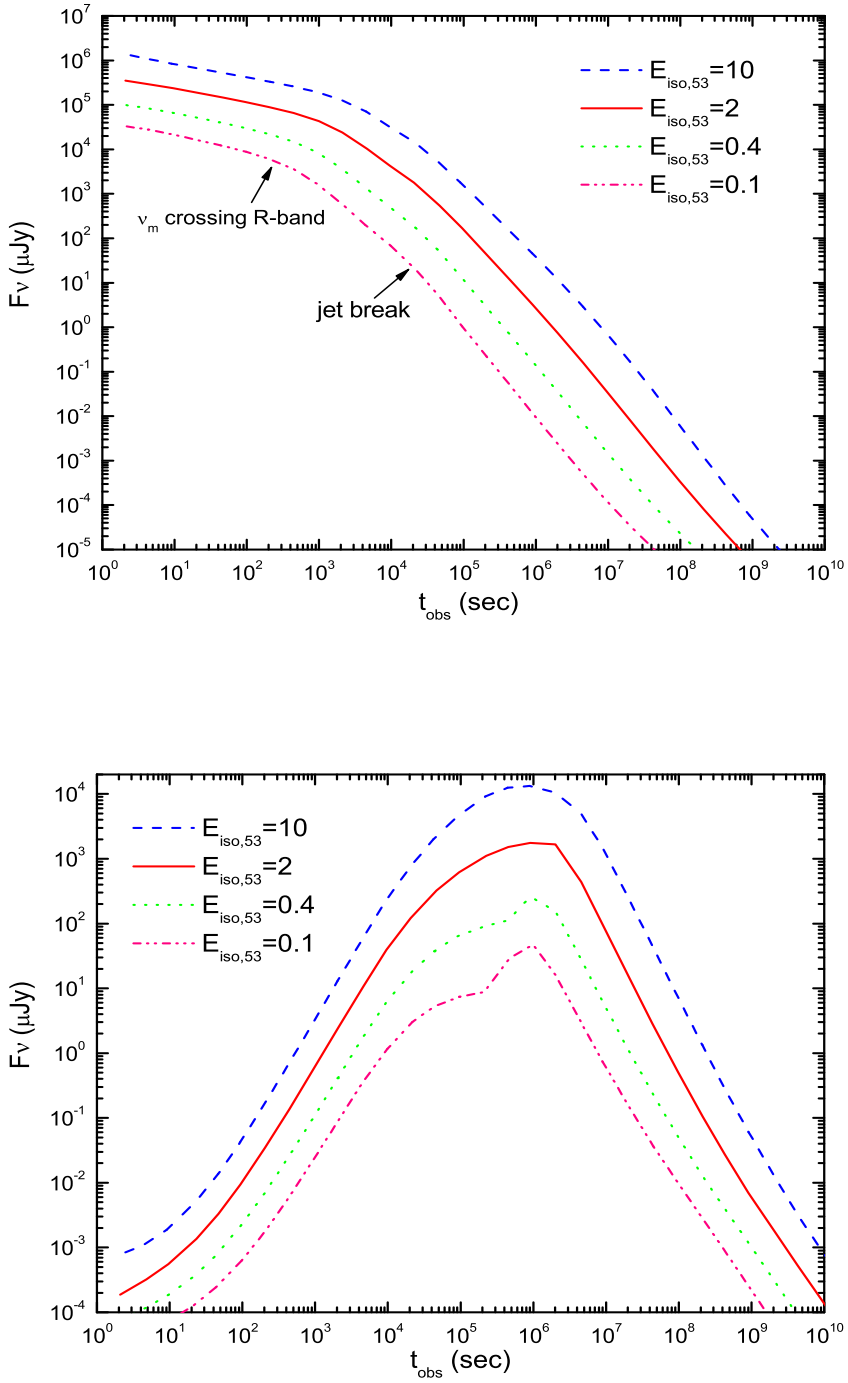

Fig. 1 Effects of the parameter $E_{\rm iso}$ on the optical ($R-$band, upper panel) and radio (4.86 GHz, lower panel) light curves. The solid line corresponds to a 'standard' jet with $E_{\rm iso} = 2 \times 10^{53}$ erg, $\theta_0 = 0.1$, $\gamma_0 = 300$, $\xi_{\rm e} = 0.1$, $\xi_{\rm B} = 0.1$, and $p = 2.2$ running into a stellar wind with $A_* = 1.0$. Other lines are drawn with only $E_{\rm iso}$ changed.

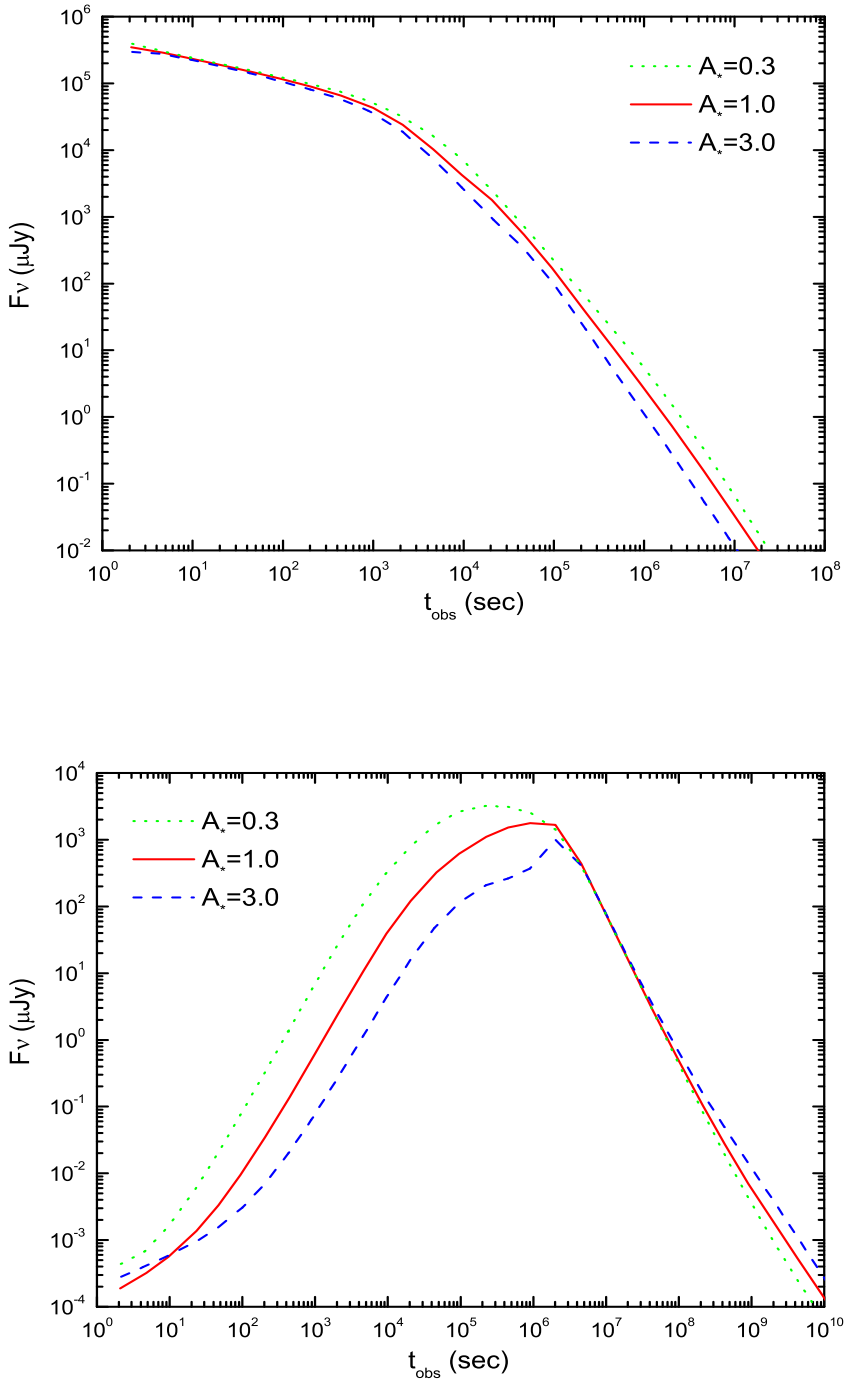

Fig. 2 Effect of the parameter A_* on the optical ($R-$band, upper panel) and radio (4.86 GHz, lower panel) light curves. The solid line corresponds to a 'standard' jet with $E_{\rm iso} = 2 \times 10^{53}$ erg, $\theta_0 = 0.1$, $\gamma_0 = 300$, $\xi_{\rm e} = 0.1$, $\xi_{\rm B} = 0.1$, and $p = 2.2$ running into a stellar wind with $A_* = 1.0$. Other lines are drawn with only A_* changed.

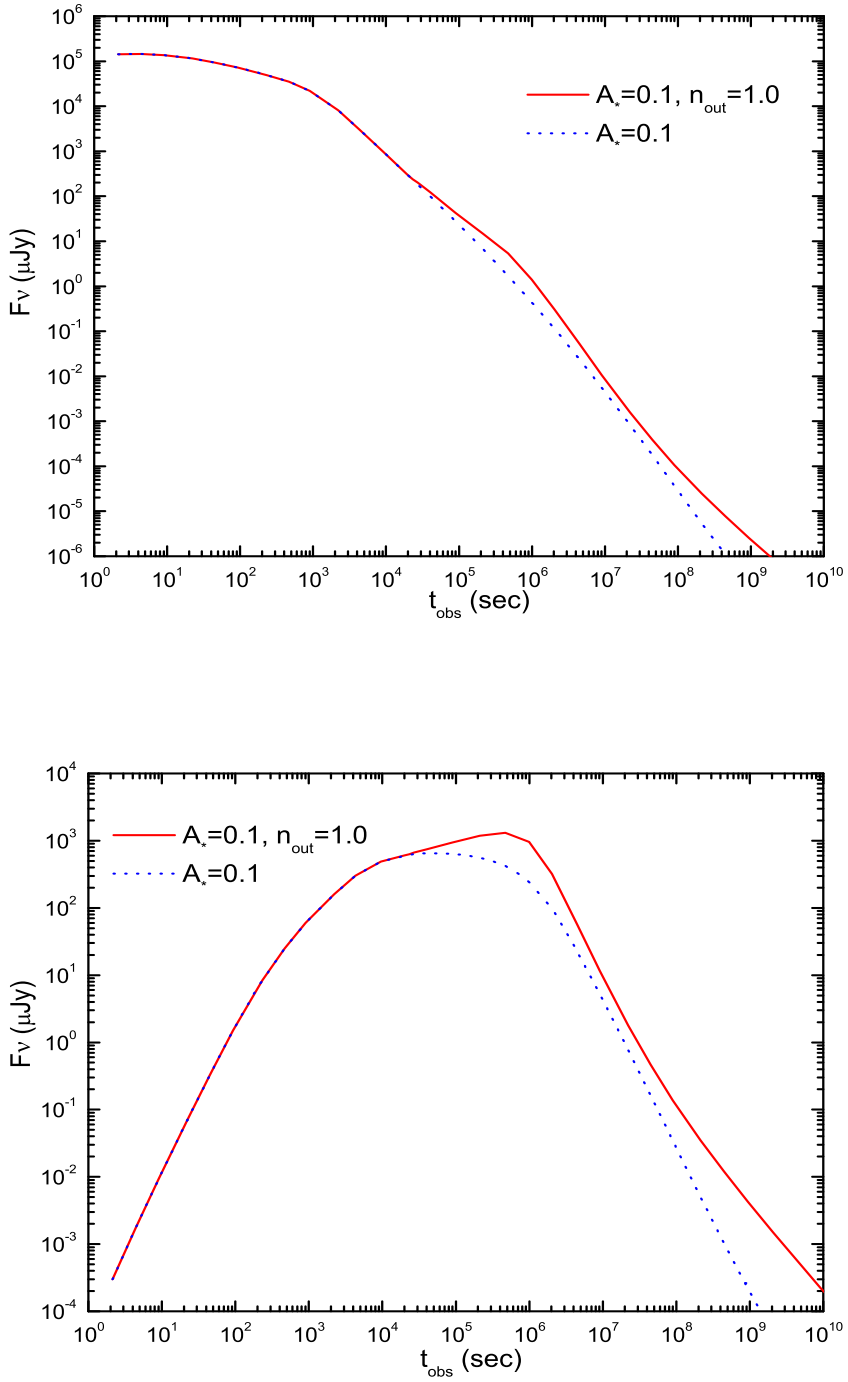

Fig. 3 Optical ($R-$band, upper panel) and radio (4.86 GHz, lower panel) afterglows from jets in a wind environment surrounded by a uniform medium. The solid line corresponds to a jet with $E_{\rm iso} = 2 \times 10^{53}$ erg, $\theta_0 = 0.1$, $\gamma_0 = 300$, $\xi_{\rm e} = 0.1$, $\xi_{\rm B} = 0.1$, and $p = 2.2$ running into a circum-stellar wind with $A_* = 0.1$ and then entering the outer uniform medium of $n_{\rm out} = 1.0$ cm^{-3} when $R > R_{\rm c} = 4 \times 10^{17}$ cm. An entire stellar wind situation is calculated (dotted line) for comparison.

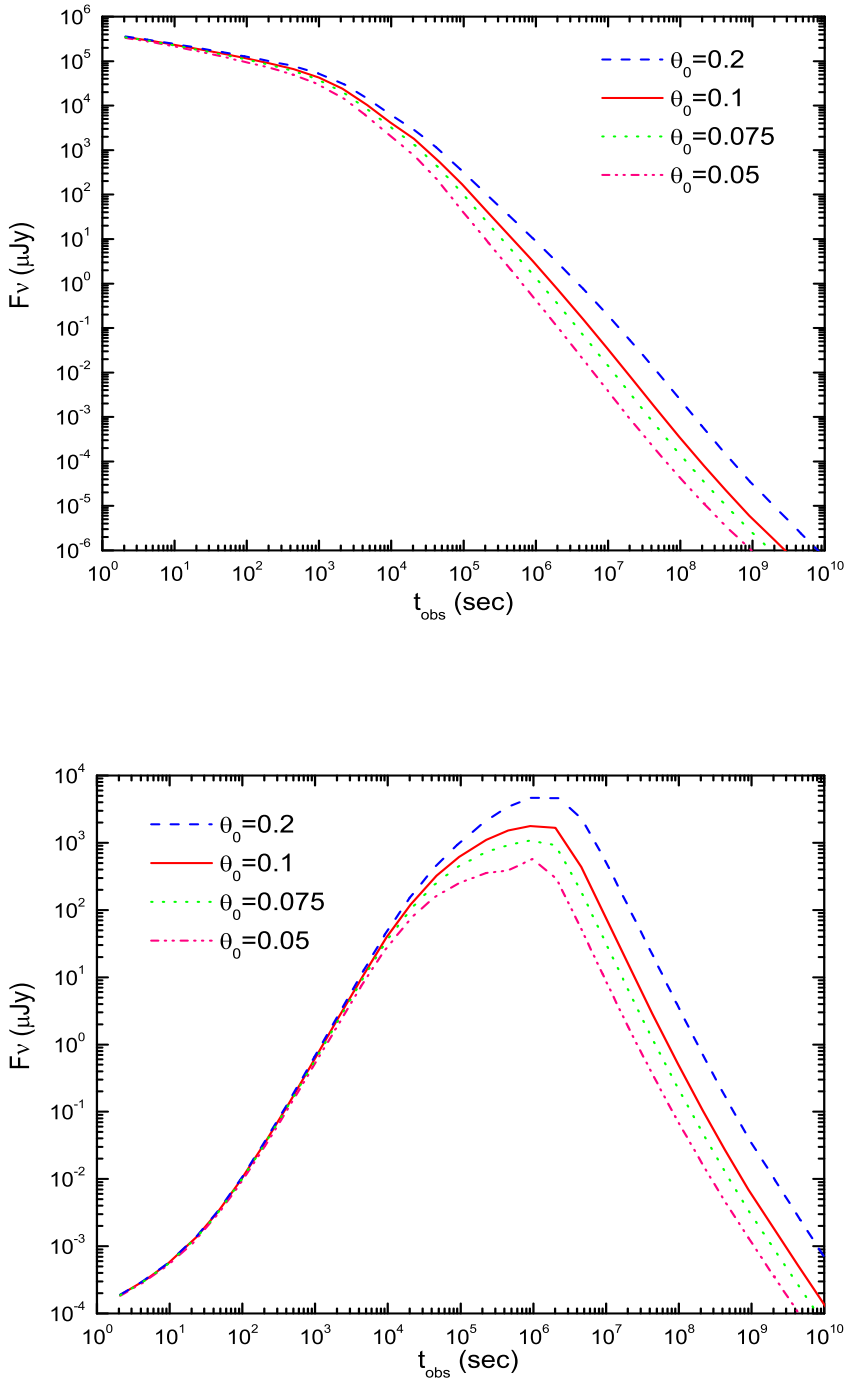

Fig. 4 Effects of the parameter θ_0 on the optical ($R-$band, upper panel) and radio (4.86 GHz, lower panel) light curves. The solid line corresponds to a 'standard' jet with $E_{\rm iso} = 2 \times 10^{53}$ erg, $\theta_0 = 0.1$, $\gamma_0 = 300$, $\xi_{\rm e} = 0.1$, $\xi_{\rm B} = 0.1$, and $p = 2.2$ running into a stellar wind with $A_* = 1.0$. Other lines are drawn with only θ_0 changed.

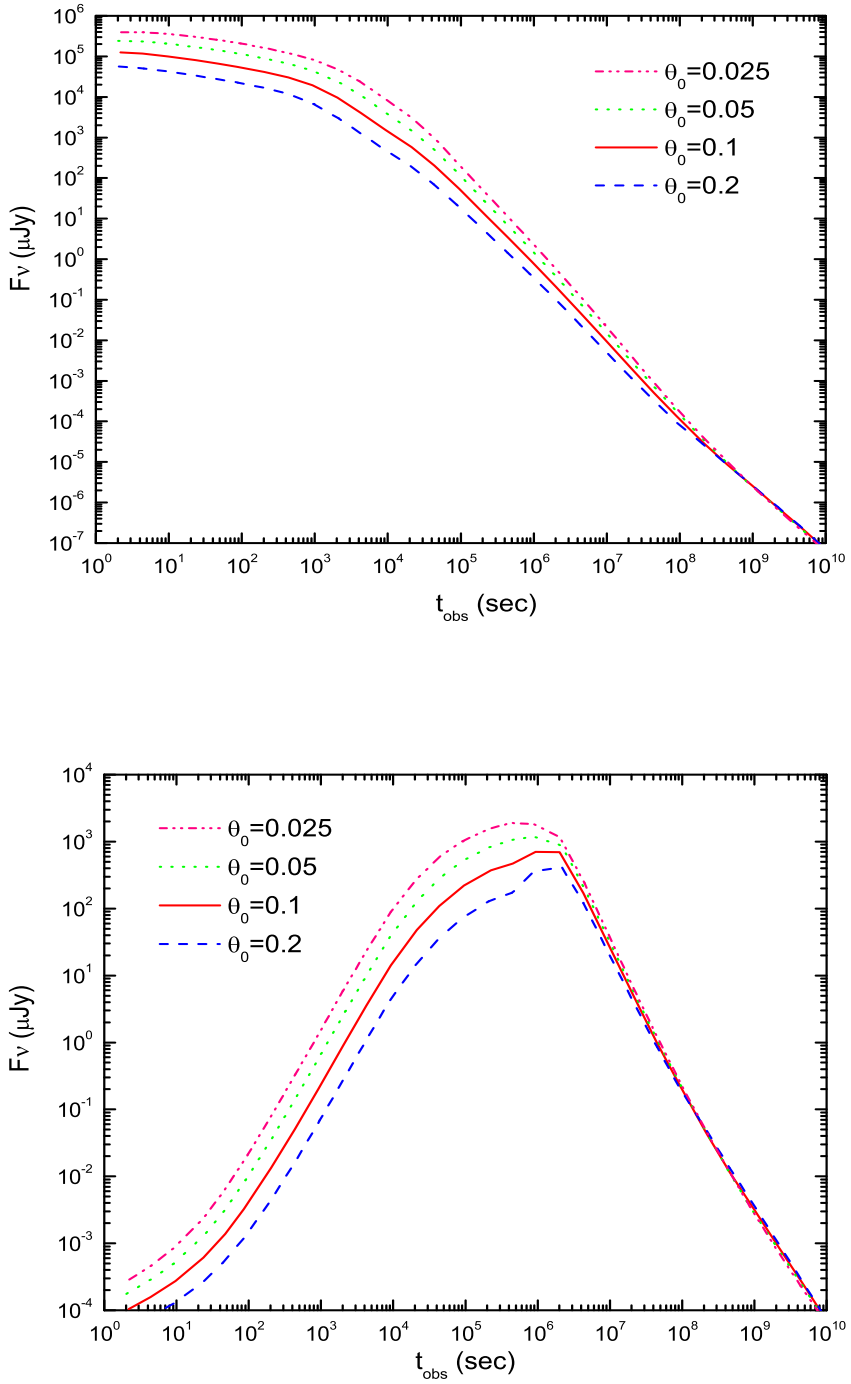

Fig. 5 Optical ($R-$band, upper panel) and radio (4.86 GHz, lower panel) afterglows from jets under the standard energy reservoir assumption, i.e. $E_{\rm j} = E_{\rm iso}\frac{\theta_0^2}{2} \equiv 2\times10^{51}$ erg. The solid line corresponds to a 'standard' jet with $E_{\rm iso} = 2\times10^{53}$ erg, $\theta_0 = 0.1$, $\gamma_0 = 300$, $\xi_{\rm e} = 0.1$, $\xi_{\rm B} = 0.1$, and $p = 2.2$ running into a stellar wind with $A_* = 1.0$. Other lines are drawn with only θ_0 changed while keeping $E_{\rm j}$ the same.

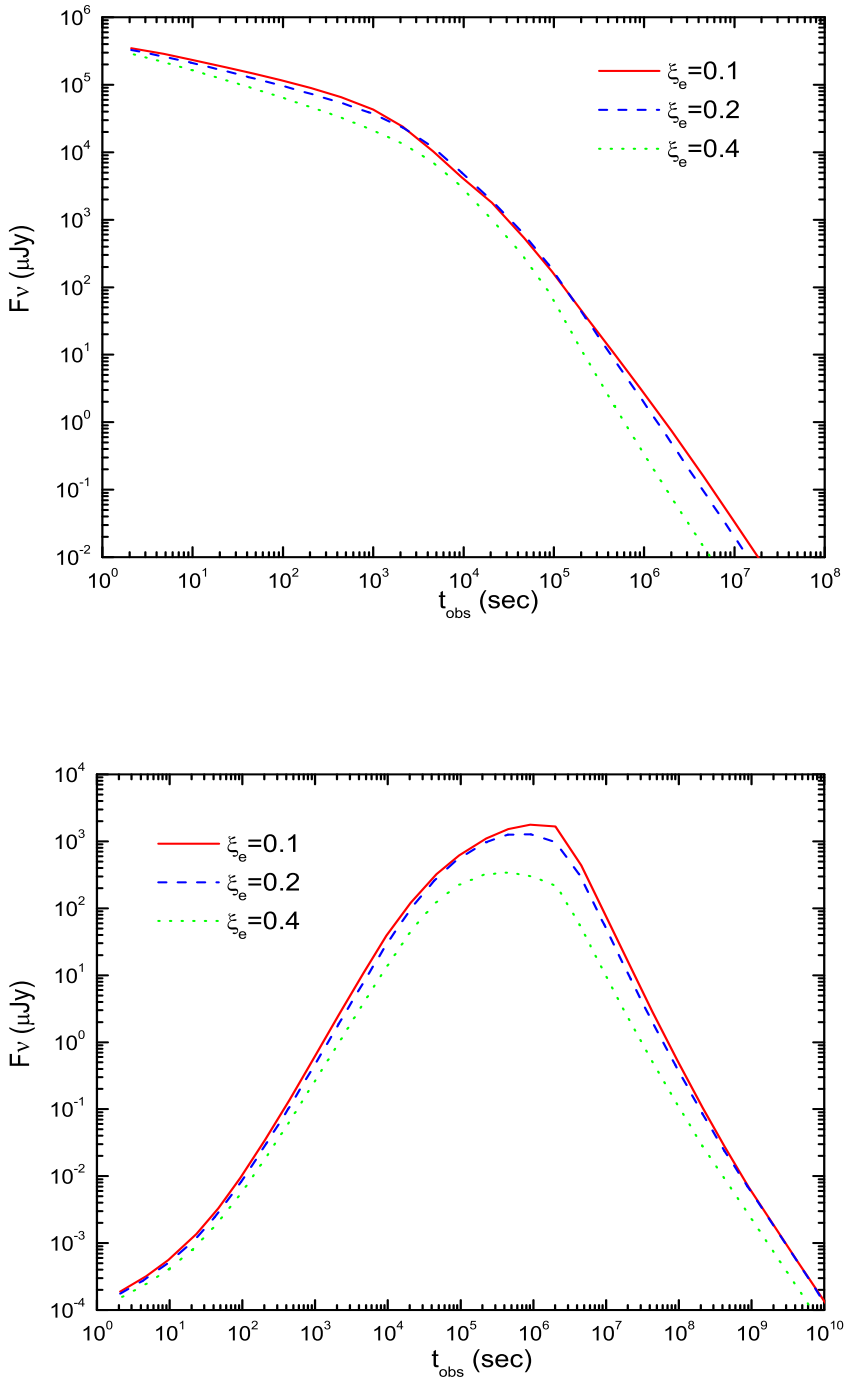

Fig. 6 Effects of the parameter $\xi_{\rm e}$ on the optical ($R-$band, upper panel) and radio (4.86 GHz, lower panel) light curves. The solid line corresponds to a 'standard' jet with $E_{\rm iso} = 2 \times 10^{53}$ erg, $\theta_0 = 0.1$, $\gamma_0 = 300$, $\xi_{\rm e} = 0.1$, $\xi_{\rm B} = 0.1$, and $p = 2.2$ running into a stellar wind with $A_* = 1.0$. Other lines are drawn with only $\xi_{\rm e}$ changed.

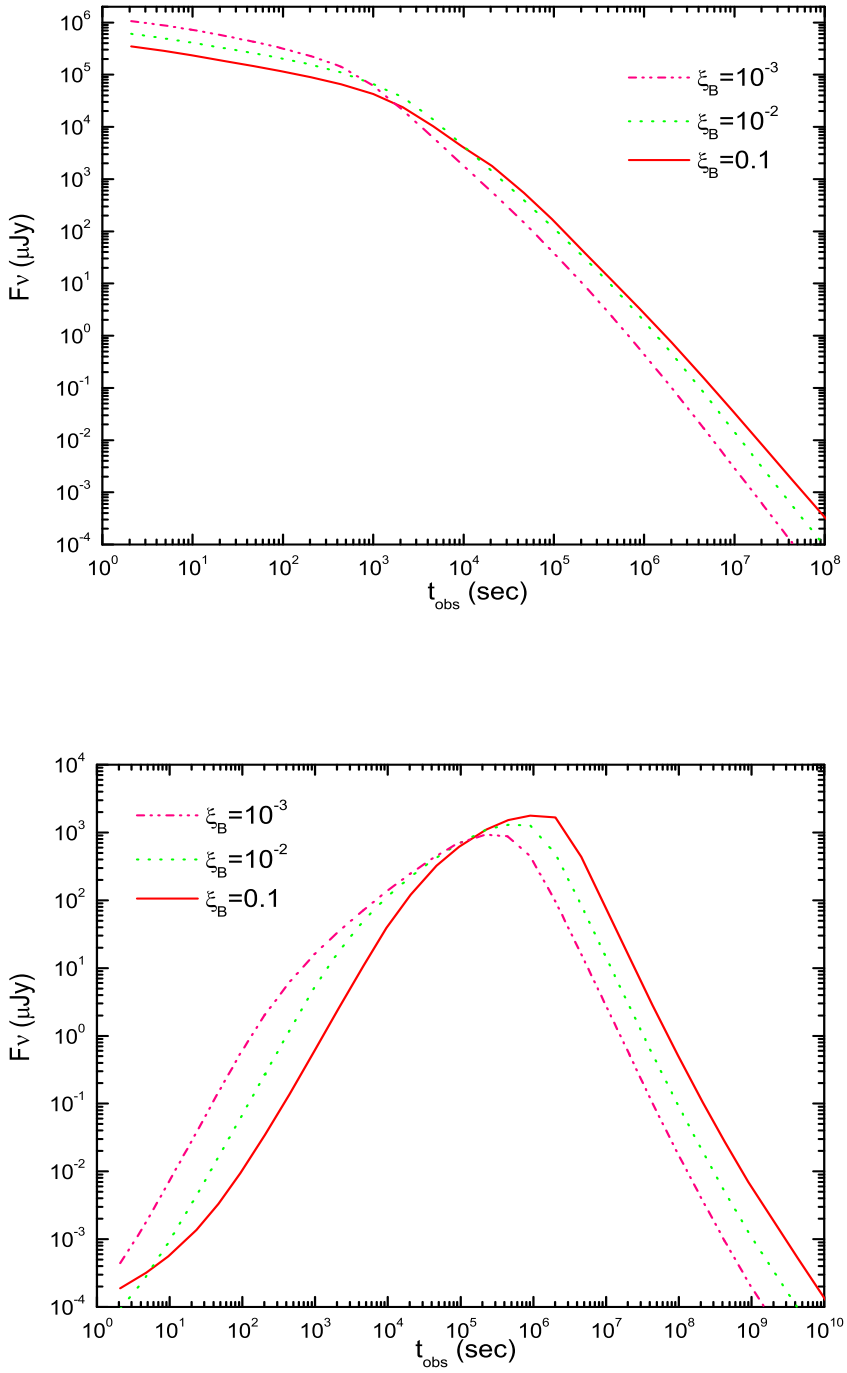

Fig. 7 Effects of the parameter $\xi_{\rm B}$ on the optical ($R-$band, upper panel) and radio (4.86 GHz, lower panel) light curves. The solid line corresponds to a 'standard' jet with $E_{\rm iso}=2\times10^{53}$ erg, $\theta_0=0.1$, $\gamma_0=300$, $\xi_{\rm e}=0.1$, $\xi_{\rm B}=0.1$, and $p=2.2$ running into a stellar wind with $A_*=1.0$. Other lines are drawn with only $\xi_{\rm B}$ changed.

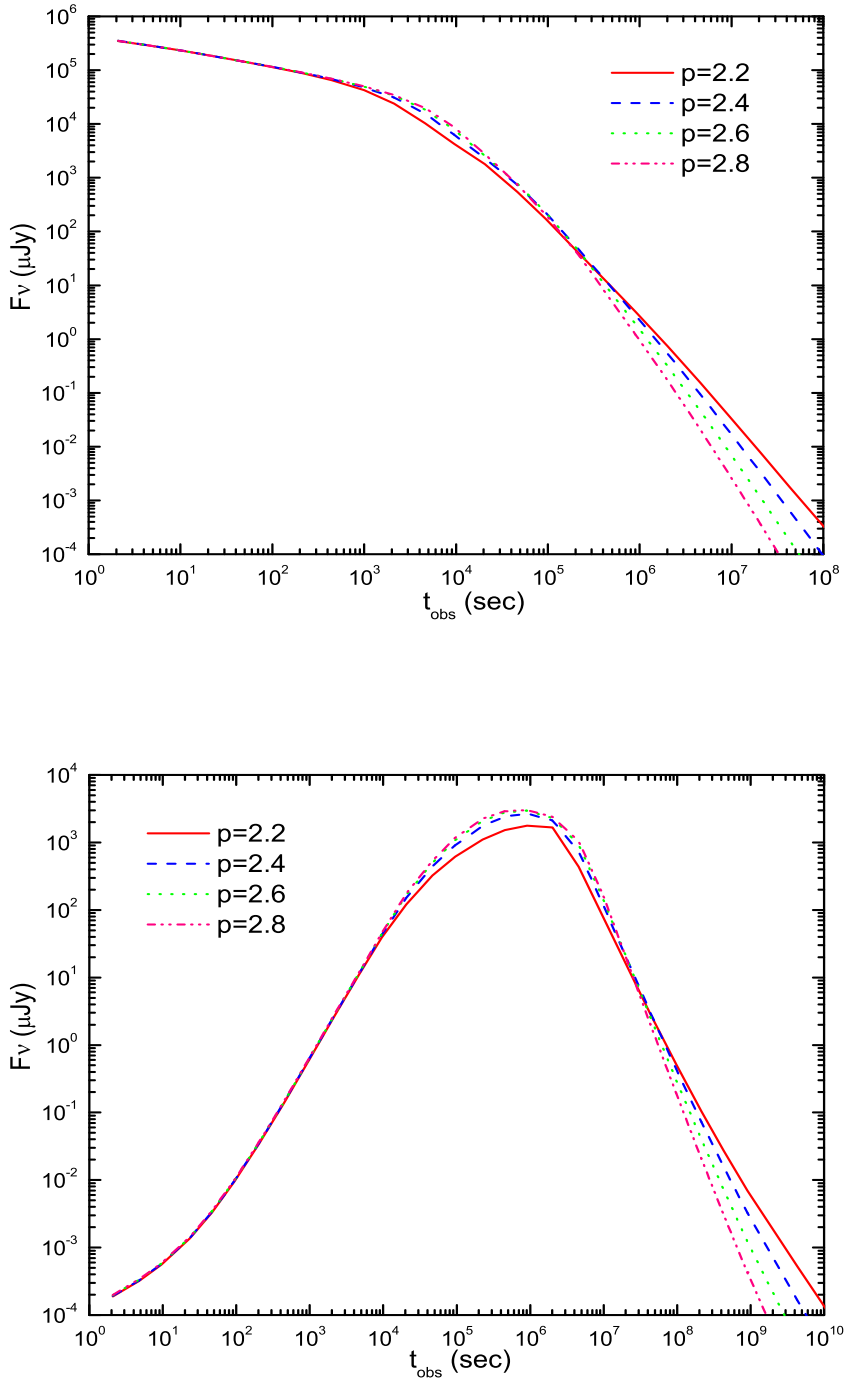

Fig. 8 Effects of the parameter p on the optical ($R-$band, upper panel) and radio (4.86 GHz, lower panel) light curves. The solid line corresponds to a 'standard' jet with $E_{\rm iso} = 2 \times 10^{53}$ erg, $\theta_0 = 0.1$, $\gamma_0 = 300$, $\xi_{\rm e} = 0.1$, $\xi_{\rm B} = 0.1$, and $p = 2.2$ running into a stellar wind with $A_* = 1.0$. Other lines are drawn with only p changed.

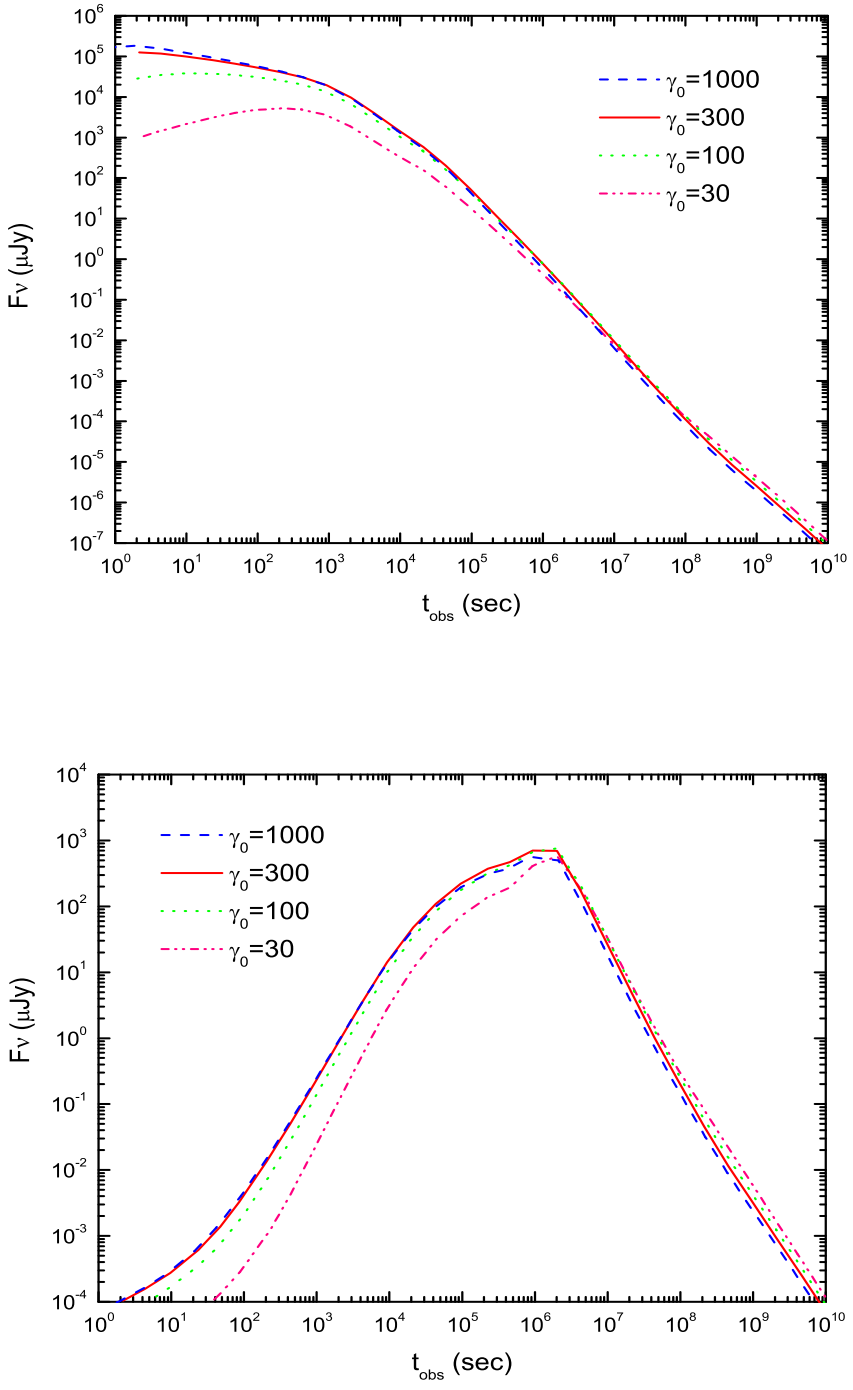

Fig. 9 Effects of the parameter γ_0 on the optical ($R-$band, upper panel) and radio (4.86 GHz, lower panel) light curves. The solid line corresponds to a 'standard' jet with $E_{\rm iso} = 2 \times 10^{53}$ erg, $\theta_0 = 0.1$, $\gamma_0 = 300$, $\xi_{\rm e} = 0.1$, $\xi_{\rm B} = 0.1$, and $p = 2.2$ running into a stellar wind with $A_* = 1.0$. Other lines are drawn with only γ_0 changed.

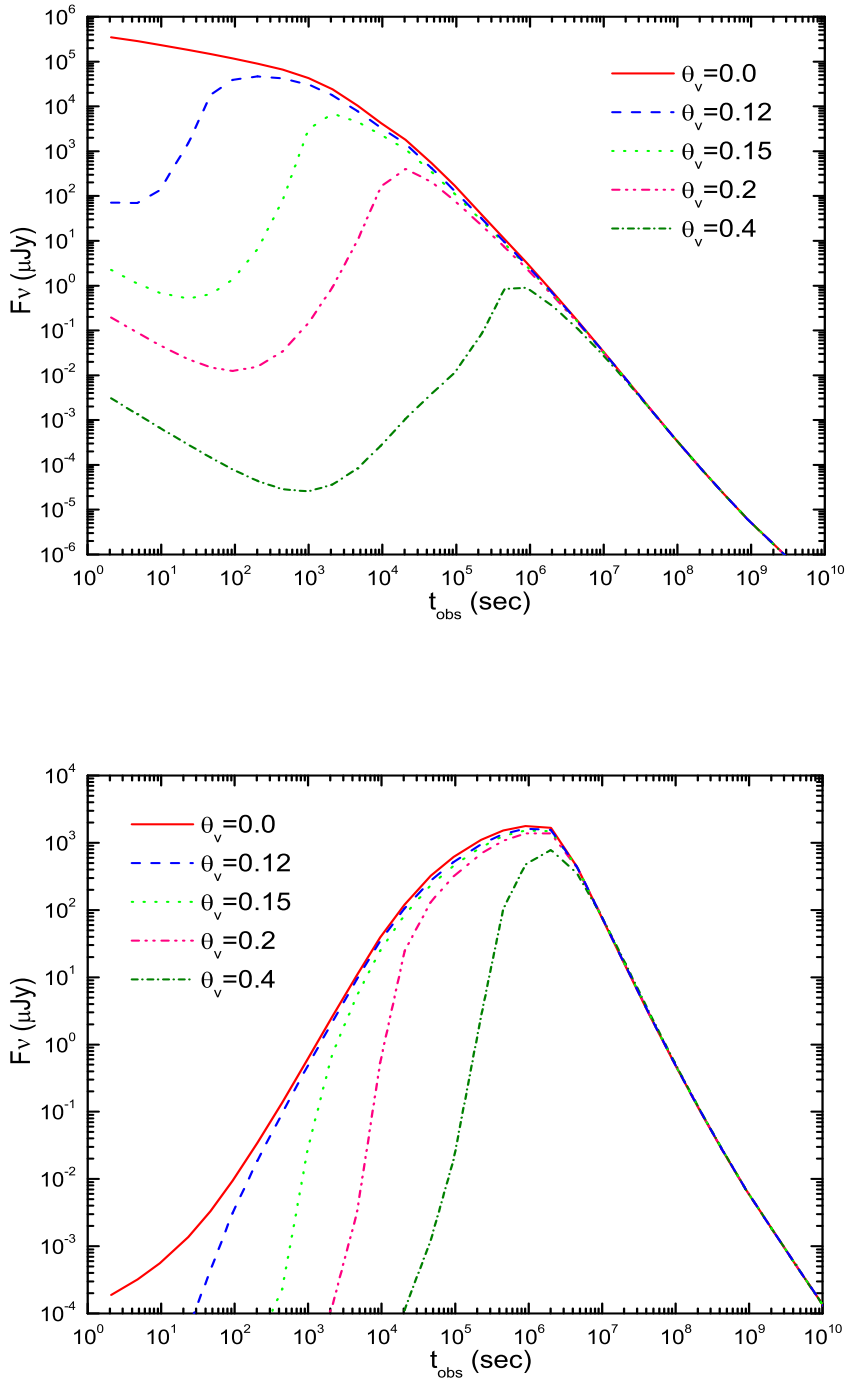

Fig. 10 Effects of the parameter $\theta_{\rm v}$ on the optical ($R-$band, upper panel) and radio (4.86 GHz, lower panel) light curves. The solid line corresponds to a 'standard' jet with $E_{\rm iso} = 2 \times 10^{53}$ erg, $\theta_0 = 0.1$, $\gamma_0 = 300$, $\xi_{\rm e} = 0.1$, $\xi_{\rm B} = 0.1$, and $p = 2.2$ running into a stellar wind with $A_* = 1.0$. Other lines are drawn with only $\theta_{\rm v}$ changed.

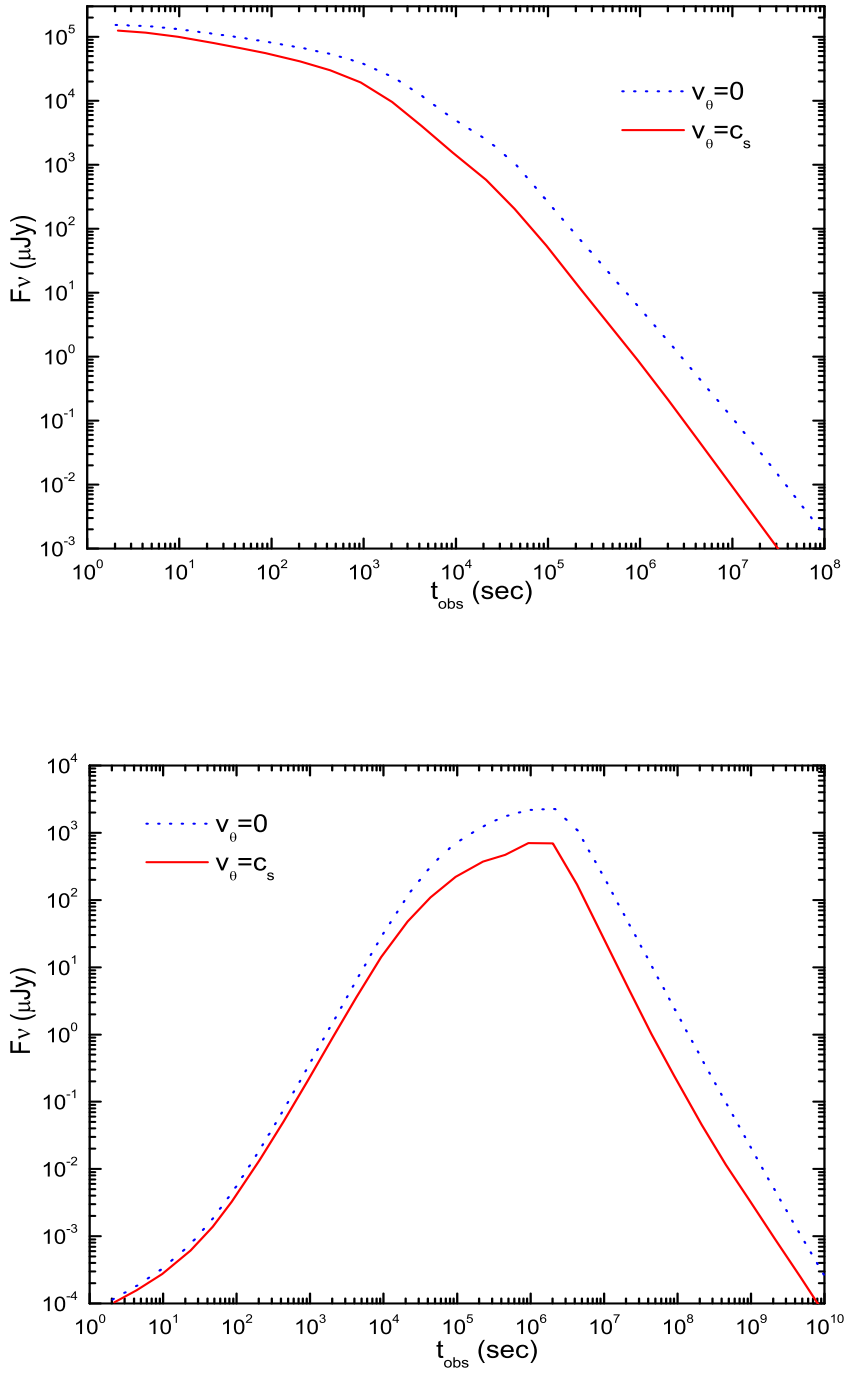

Fig. 11 Effects of lateral expansion velocity v_θ on the optical ($R-$band, upper panel) and radio (4.86 GHz, lower panel) light curves. The solid line corresponds to a 'standard' jet with $E_{\rm iso}=2\times10^{53}$ erg, $\theta_0=0.1$, $\gamma_0=300$, $\xi_{\rm e}=0.1$, $\xi_{\rm B}=0.1$, and $p=2.2$ running into a stellar wind with $A_*=1.0$, with $v_\theta=c_{\rm s}$. The dotted line corresponds to no lateral expansion, i.e. $v_\theta=0$.